AGU ADVANCING EARTH AND SPACE SCIENCE

Water Resources Research

RESEARCH ARTICLE
10.1029/2022WR032116

Analysis of the Vibration Modes of Impact Geoplates and Implications for Bedload Flux and Grain Size Measurements

M. Portogallo[1,2,3], S. Simoni[1], G. Vignoli[2,4], and W. Bertoldi[3]

[1]Mountain-eering srl, Bolzano, Italy, [2]CISMA srl, Bolzano, Italy, [3]Department of Civil, Environmental and Mechanical Engineering, University of Trento, Trento, Italy, [4]Now at Penta Automazioni Industriali srl, Molinella, Italy

Key Points:

- Fourier and wavelet analysis of the geophone signal highlights the plate vibrates with a fundamental frequency in the range of 300–400 Hz
- Amplitude of the fundamental mode depends on particles mass and is not affected by flow conditions, whereas the number of impacts is
- Amplitude of the main vibration mode is related to grain size, but also pebble shape has a significant role

Supporting Information:

Supporting Information may be found in the online version of this article.

Correspondence to:

W. Bertoldi,
walter.bertoldi@unitn.it

Citation:

Portogallo, M., Simoni, S., Vignoli, G., & Bertoldi, W. (2022). Analysis of the vibration modes of impact geoplates and implications for bedload flux and grain size measurements. *Water Resources Research*, *58*, e2022WR032116. https://doi.org/10.1029/2022WR032116

Received 31 JAN 2022
Accepted 13 SEP 2022

Abstract Seismic geophones have been frequently used in combination with metal plates to indirectly estimate bedload flux in gravel bed mountain rivers. This indirect method has been calibrated with direct measurements in several conditions and proved effective to provide relevant information on spatial and temporal scales otherwise impossible to explore. Notwithstanding, a detailed description of the vibration modes of the plate is still lacking, limiting the possibility to interpret the signal. Here, we report on two sets of experiments where we explored the geoplate response in terms of frequency and amplitude of different vibrational modes. A first set of dry experiments was designed to investigate the variability of the signal as a function of the impact location on the plate. A second set reproduced standard flow conditions, with single pebbles transported by the flow. Results highlighted the occurrence of two main vibration modes, with a first rapid phase (about 5 ms) characterized by higher frequencies, and a second longer and more stable phase of vibration with a frequency in the range of 300–400 Hz. The signal of single impacts showed a good correlation with pebble mass, with only the number of impacts on the plate depending on the flow conditions. The evaluation of the grain size is a challenge given the variability of the signal generated by similar impacts. We propose a filtering strategy to improve grain size estimation. Our analysis shows that a more detailed understanding of the vibrational modes helps identifying best practices for an improved signal acquisition and elaboration.

Plain Language Summary Vibration produced by sediments transported on the riverbed can be used to indirectly estimate sediment flux in rivers. A commonly used method involves the installation of metal plates on the riverbed. Their vibration is measured by geophones and converted into metrics related to sediment flux. In this work, we performed laboratory experiments to better understand the vibration modes of the plate, measuring the frequency and amplitude of the different harmonics through a Fourier analysis. In a first set of experiments, we investigated the variability of the signal as a function of the hitting spot on the plate, in dry conditions. A second set reproduced standard flow conditions, with single particles transported by the flow. Results showed that the plate vibrates mainly with its natural frequency (about 350 Hz), with higher frequencies related to higher vibration modes damping very rapidly. Particles hit the plate one or more times, generating impacts with amplitudes related mainly to their mass, whereas the number of impacts also depends on the flow conditions. Filtering the impacts as a function of their vibration spectra may result in more accurate relationships between the recorded signal and sediment flux and may help designing improved signal acquisition and elaboration tools.

1. Introduction

The development of indirect bedload flux measurement techniques represents a potential game changer in river science. The possibility of having spatially and temporally detailed estimates of the sediment flux in rivers may indeed largely improve and change our understanding of fluvial processes with implications for flood risk assessment, as well as river restoration schemes and habitat modeling. The lack of accurate sediment transport data is one of the major constraints when addressing a variety of river management problems, including flood defense and river restoration, and at spatial scales from the watershed to the river reach (Wilcock, 2001).

Direct bedload measurements are often challenging and costly, and only rarely do they provide acceptably accurate data over large discharge events, which tend to mobilize the highest bedload (Vericat et al., 2006). Moreover, traps and samplers are not designed to capture and take into account the inherent stochastic nature of sediment transport processes (Recking et al., 2010). On the other hand, indirect measurements provide a continuous monitoring of sediment flux, including at high flows. Different techniques have been proposed, aiming at

measuring (a) the sound emitted by the movement of particles (Geay et al., 2020); (b) the vibration induced by the particles hitting the riverbed, colliding with each other, or hitting specifically designed structures such as metal pipes or plates (Gray et al., 2010; Rickenmann, 2017; Schmandt et al., 2013); or (c) bedload velocity using acoustic Doppler profilers (Rennie et al., 2002). Acoustic and seismic sensors produce electrical signals, which are then analyzed in terms of amplitude, frequency, or simply number of impulses, and transformed into sediment load and/or grain size by means of calibration obtained from direct estimates.

Acoustic sensors record the sound waves generated by the moving particles, using high-frequency acquisition rates, up to 100 kHz (Tsakiris et al., 2014). Several studies demonstrated that the analysis of the complete spectral waveform, in terms of spectral power density and dominant wavelengths, can produce accurate information on bedload flux and its grain size (e.g., Geay et al., 2020; Petrut et al., 2018; Tsubaki et al., 2017). In particular, large particles produce a signal characterized by higher amplitudes and lower frequencies. So far, this promising technique is being used mainly at research level, because of a more complex field setup, data acquisition, and analysis.

In recent years, devices such as the pipe hydrophones, often called Japanese pipe (Mizuyama et al., 2010) and the impact plate system, often called the Swiss Geophone Plate (Rickenmann & McArdell, 2007), have been installed in many rivers in Japan and in the European Alps, allowing for a continuous survey of bedload and the development of sediment rating curves. The success of these devices lays also in (a) their relatively easy and resistant setup, as they are fixed to retention structures or other concrete structures; and (b) a rather simple data acquisition and analysis, as generally the signal is reduced to the count of impulses, that is, the number of times the signal exceeds a fixed threshold. This metric is easy to compute and store and has been demonstrated to be a good proxy of the sediment load (Mao et al., 2016; Rickenmann et al., 2012; Soar & Downs, 2017). Studies carried out in controlled environments and with physical modeling showed that additional parameters such as the amplitude and frequency of the acquired signal can provide more detailed information, including the grain size of transported particles (Barrière et al., 2015; Nicollier, Antoniazza, Rieckenmann, et al., 2022; Wyss et al., 2016a, 2016b).

More recent studies aimed at investigating the response of impact plates and in particular the variability of the calibration coefficients relating the number of impulses to the bedload flux. Antoniazza et al. (2020) showed that the amplitude of the signal measured by a geophone strictly relates to the kinetic energy of the hitting particle. However, they pointed out the significant role of vibration propagation across plate arrays, with non-negligible effects on the number of recorded impulses in the case of multiple plates attached to the same structure. Filtering these spurious impacts strongly enhances the calibration of the geoplate (Nicollier, Antoniazza, Rieckenmann, et al., 2022). Nicollier et al. (2021) performed a series of laboratory experiments with single-grain size and mixed-grain size distributions highlighting a strong variability of the calibration parameters with grain size.

These recent findings underline the need to better understand the vibration mechanics of the impact plates, in terms of dominant vibration modes and associated energy. In this paper, we report on experiments on an impact plate with geophone, aiming at understanding its vibration response when subject to hits by particles of different sizes and masses. The experiments were firstly carried out in dry conditions, and then in a flume setup, recording the full signal of the geophone at high frequency.

The specific objectives of the work are: (a) to understand the response of the impact plate in terms of frequency and amplitude of its vibration harmonics, as a function of the particle mass or diameter, and also as a function of the distance of the impact point from the plate's center; (b) to identify which parameters are better related to particle mass or diameter, and which parameters minimize the measured variability induced by a different flow field; (c) to explore the possibility to estimate sediment grain size from the recorded signal. Results will also help identifying best practices in signal acquisition and analysis.

2. Materials and Methods

2.1. The Geophone Plate

We used a measuring device similar to that developed by Rickenmann et al. (2012). The seismic instrument consists of a vertical geophone produced by the company “Pasi” mounted below the center of a 10 mm thick steel plate with sides 494 and 358 mm long. The weight of the plate is 13.1 kg. The plate is supported by a metal box, which also protects the geophone. Between the plate and the box, there is a 21 mm thick elastomer gasket, which acts as a damper of the vibrations induced by impacting particles and isolates the geophone from external noise sources (Figure 1a). This gasket frames the box, has a width of 50 mm and weighs 2.4 kg. The plate is fixed to the

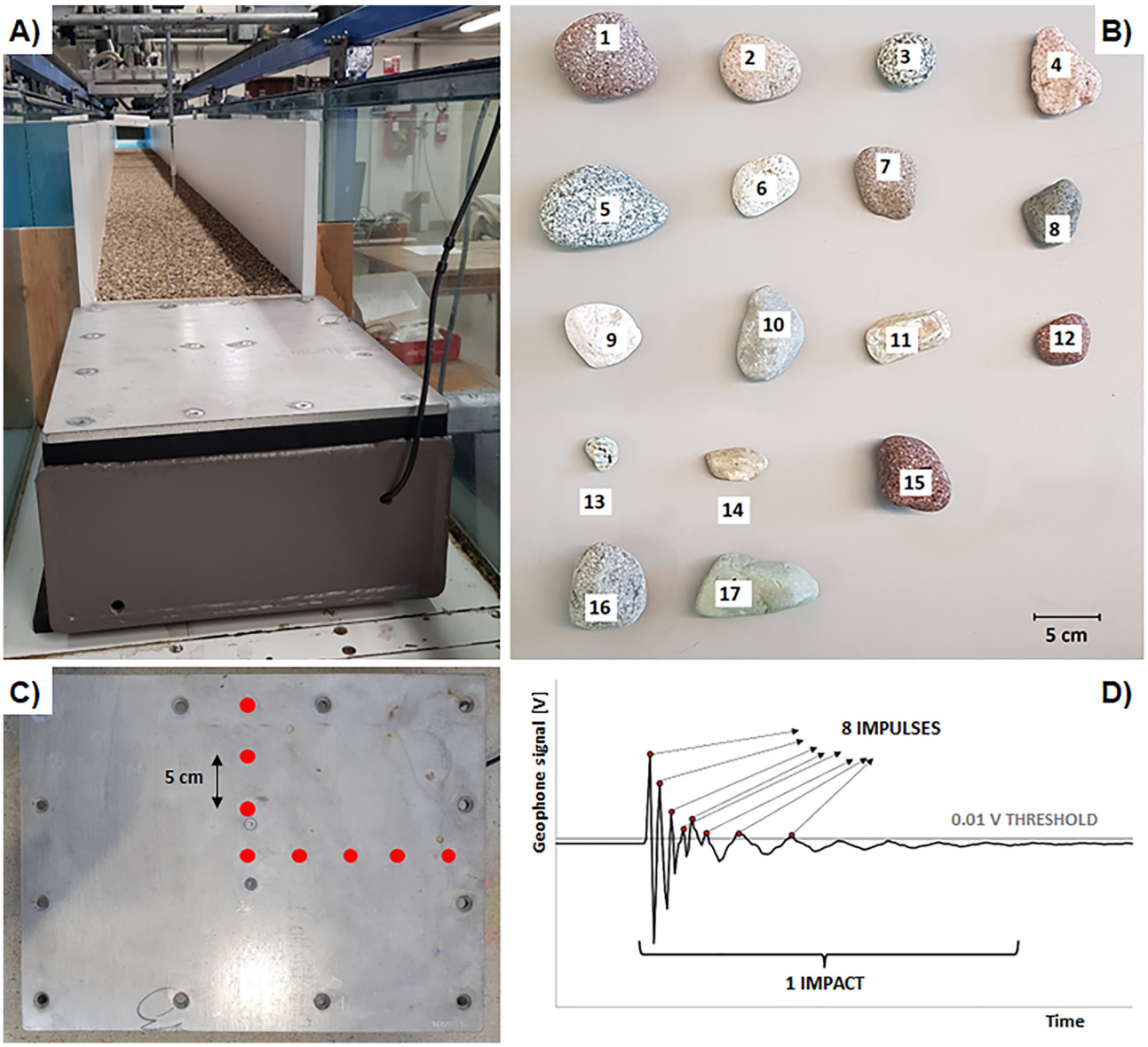

Figure 1. (a) Image of the flume used for the flow experiments with the gantry and the point gauge; (b) the 17 pebbles used in the experiments; (c) the metal plate and the eight fixed points (in red) used for the dry experiments; (d) a typical geophone signal with the definition of impulse and impact.

box with 12 screws uniformly distributed around the perimeter of the plate (Figure 1c); the screws were tightened with a torque of 2.8 N · m, to avoid excessive compression of the elastomer. The plate was mounted with both the long axis parallel (as in Figure 1a) and perpendicular to the flow (as normally in the field). No significant difference was highlighted and only the results for the runs with the plate mounted as in the field are reported in the following.

The geophone signal was sampled by a datalogger at a predetermined frequency. The acquisition and data storage were managed by a Raspberry Pi single-board computer. In most of the experiments, the signal was recorded with a sampling frequency of 10 kHz, in accordance with Rickenmann et al. (2012). In a specific set of runs (see below), the signal was sampled at higher frequency, namely 30 kHz.

2.2. Dry Experiments

The first set of experiments was performed in dry conditions, to investigate the variability of the signal associated with different impact points. For this setup, we used a 64 g steel sphere, which was dropped from a height of

Table 1
Characteristic Dimensions of the Natural Pebbles Used in the Flow Experiments

Particle id	d_1 [mm]	d_2 [mm]	d_3 [mm]	d_{sphere} [mm]	Mass [g]	Shape factor [–]
1	74.6	65.7	63.9	67.9	510	0.91
2	72.2	50.2	40.3	52.6	227	0.67
3	51.5	51.5	43.3	48.6	168	0.84
4	78.6	60.6	28.5	51.4	177	0.41
5	108.0	75.3	53.0	75.5	559	0.59
6	62.7	45.1	37.2	47.2	145	0.70
7	57.9	54.8	33.4	47.3	164	0.59
8	62.9	50.3	37.8	49.2	148	0.67
9	67.6	57.1	40.1	53.7	173	0.65
10	83.8	55.5	36.2	55.2	216	0.53
11	75.5	38.6	37.2	47.7	164	0.69
12	51.1	42.1	32.1	41.0	92	0.69
13	31.2	26.2	25.8	27.6	31	0.90
14	54.2	25.0	25.0	32.4	48	0.68
15	59.7	54.4	54.4	56.1	309	0.95
16	75.2	59.8	44.1	58.3	372	0.66
17	106.5	43.6	37.3	55.7	346	0.55

Note. d_1, d_2, and d_3 represent three orthogonal axes of the pebble, from the larger to the smaller. d_{sphere} is the equivalent diameter of a sphere with the same volume. The Corey shape factor is computed as $d_3/(d_1 d_2)^{1/2}$.

20 cm on 8 different points on the plate (see Figure 1c). The sphere hit the plate only once at each throw and was then stopped. The experiment was repeated 50 times for each point of the plate. In a further set of experiments, we tested the effect of four different supporting configurations of the plate: (a) fixed with elastomer (as in all the other tests); (b) simply supported on the elastomer; (c) fixed without elastomer; and (d) simply supported without elastomer. In this case, we tested three positions on the plate, with the sphere hitting the center of the plate and two positions at 10 cm from the center in both directions.

These simple experiments were used to better understand the vibration signal associated with each particle hit. Therefore, we also sampled the signal with a higher acquisition rate, to highlight the occurrence of higher frequencies.

2.3. Flow Experiments

A second set of experiments was performed reproducing typical field conditions when sediments transported by the flow hit and rolled on the plate. Experiments were carried out in the Hydraulics Laboratory of the Department of Civil, Environmental, and Mechanical Engineering of the University of Trento. The flume consisted in a straight channel, 7 m long, with a rectangular cross-section of 0.3 m width, and a constant slope adjustable through a hydraulic piston. The channel was made of smooth PVC, with heterogeneous sand (with a 90th percentile diameter equal to 2 mm) glued on the bed to increase the roughness. Bed roughness was added to ensure the introduced pebbles moved also by rolling and saltation, not only by sliding, as was more likely on a smooth surface. Water discharge was provided by a closed hydraulic circuit and ranged between 10 and 40 l/s. Upstream of the channel, a calm basin facilitated the establishment of uniform and steady flow and dissipated the turbulence generated by the closed hydraulic circuit. Flow depth was measured by a point gauge mounted on a moving gantry (see Figure 1a). The geophone plate was located immediately downstream of the channel outlet, at an elevation 5 mm lower than the channel bed, to prevent sediment from stopping before the plate. The metal box supporting the plate was placed on a soft rubber layer, to avoid spurious oscillations generated by the entire structure. Downstream of the plate, a vibration-absorbing sponge stopped the particles, preventing additional vibration and signal disturbances. Figure 1a shows an image of the flume.

For these experiments, we used a set of 17 natural pebbles, with different sizes and shapes (see Figure 1b). Mean diameters of the pebbles ranged approximately from 25 to 75 mm, and mass ranged from 31 to 559 g. Table 1 reports the dimensions of each pebble. In particular, the size of the pebbles is described by the diameter along three orthogonal axis, from the longest to the shortest (d_1, d_2, and d_3, respectively) and by the diameter d_{sphere}, of an equivalent sphere with the same volume, computed as the cube root of the product of the three diameters d_1, d_2, d_3. The shape of the pebbles is quantified by the Corey shape factor, computed as $d_3/(d_1 d_2)^{1/2}$, which tends to 1 for a perfect sphere and decreases for elongated or platy pebbles. The range of grain size was determined by the physical constraints of the setup. The lower limit was set by the ability of the geoplate to detect hitting particles, which is about 20 mm, according to the literature (Rickenmann et al., 2012). The upper limit of the range was set by the maximum discharge of the flume, and therefore by the maximum diameter that the flow is able to transport.

We tested five different flow configurations, changing the discharge and the longitudinal slope, to reproduce different combinations of flow depth and velocity. Hydraulic conditions are reported in Table 2.

For the five different flow conditions, each of the 17 natural pebbles was individually introduced in the flume, approximately 6 m upstream of the geoplate and was transported by the flow, hitting the plate on 1 or more points. Each run was repeated 10 times, to quantify the intrinsic variability of the process. In total, we performed 850 runs. During each run, the geophone signal was sampled and stored at 10 kHz.

Table 2
Hydraulic Conditions of the 5 Flow Configurations Used in the Flow Runs

Flow run	Discharge [l/s]	Slope [m/m]	Average depth [m]	Average velocity [m/s]	Froude number [−]
F1	13	0.05	0.035	1.24	2.12
F2	20	0.05	0.047	1.42	2.09
F3	23.5	0.02	0.064	1.22	1.54
F4	33.6	0.02	0.08	1.40	1.58
F5	38.8	0.02	0.086	1.50	1.63

Note. Velocity and Froude number are computed from the other measured data.

2.4. Data Analysis

In this paper, we clearly distinguish between impacts and impulses. An impact identifies the whole signal generated when a particle hits the plate, whereas an impulse identifies any occurrence where the geophone signal crosses a given threshold (see also Figure 1d). An impact is therefore likely to contain multiple impulses. We recall here that the number of impulses is the most used parameter in bedload plates applications, although it disregards most of the information included in the signal.

The geophone signal, measured in Volts, was analyzed to identify and characterize the effect of each impact of the pebbles on the plate. When hitting the plate, pebbles bounced at least once, and in most cases several times, therefore producing one or more impacts. The experiment setup and the use of single pebbles for each run, allowed for an easy recognition and separation of all the impacts. The 10 kHz signal of each impact was extracted from the continuously recorded signal. Starting point of each impact was identified automatically looking for sharp increases in the signal derivative. A time window of 50 ms was considered for each impact.

Similarly to what has been done in the literature, we computed the number of impulses as the number of times the raw signal exceeds a defined threshold (0.1 V, as in Rickenmann et al., 2012), for each impact (or packet as defined by Wyss et al., 2016a; Nicollier et al., 2021). We also computed the number of impacts for each run and the total number of impulses for each run. In addition, we computed the amplitude of the maximum peak of each impact (in V) and the integral of the absolute value of the signal (measured in V s), over the time period of each impact, which can be considered a proxy for the energy of the impact (Belleudy et al., 2010; Tsakiris et al., 2014).

The geophone signal of each impact was also analyzed through a Fast Fourier Transform algorithm, to identify the main harmonics and to quantify their frequency and amplitude. This was computed as twice the absolute value of the single-sided FFT estimate normalized by the length of time series. Moreover, for a selection of experiments, a wavelet analysis was performed, to better characterize the different frequencies and their temporal variability. The Morse wavelet transformation was applied, using the Matlab function "cwt."

3. Results

3.1. The Geoplate Signal

The signal produced by a single impact on the plate appears as an oscillation that is rapidly damped (see Figures 2a and 2c). The total duration of each impact is about 40 ms. In general, it can be characterized by a first part with higher frequency and amplitude, lasting approximately 5 ms, followed by a second part, which is generally more regular and shows a sequence of damped oscillations with a decreasing amplitude and a lower frequency. The background noise is very small compared to the signal, therefore filtering is not necessary.

In Figure 2, we compare the average signal produced by eight identical replicas of the metal sphere hitting the center of the plate, changing the acquisition frequency from 10 kHz in Figure 2a to 30 kHz in Figure 2c. The comparison highlights that the 10 kHz frequency is sufficient to sample also the first phase, as the largest significant frequency is less than 2.5 kHz. However, the signal in the first phase is more variable, as quantified by the coefficient of variability (ratio of the standard deviation to the mean for each data point) computed for the eight replicas. In the first phase, with an acquisition frequency of 10 kHz, the coefficient of variability ranges from 0.5 to 2, whereas for the second phase, it oscillates about 0.1. For the signal recorded at 30 kHz, the coefficient of variability is more uniform, oscillating at about 0.3. The comparison between Figures 2b and 2d shows that increasing the acquisition rate from 10 to 30 kHz does not change the outcome of the analysis, as there is no significant harmonic with a frequency higher than 2.5 kHz.

The Fourier analysis of these signals reveals a clear peak at about 300–400 Hz, followed by several combined peaks in the range from 1,000 to 2,500 Hz (see Figures 2b and 2d, for the acquisition frequency of 10 and 30 kHz, respectively).

The different vibration modes are more clearly separated by the wavelet analysis, reported in Figure 3. Results show that the first phase, spanning the first 5 ms, is characterized by higher frequencies, with a high magnitude, and damps rapidly. The longer second phase, lasting up to 30 ms, is a more regular oscillation, characterized

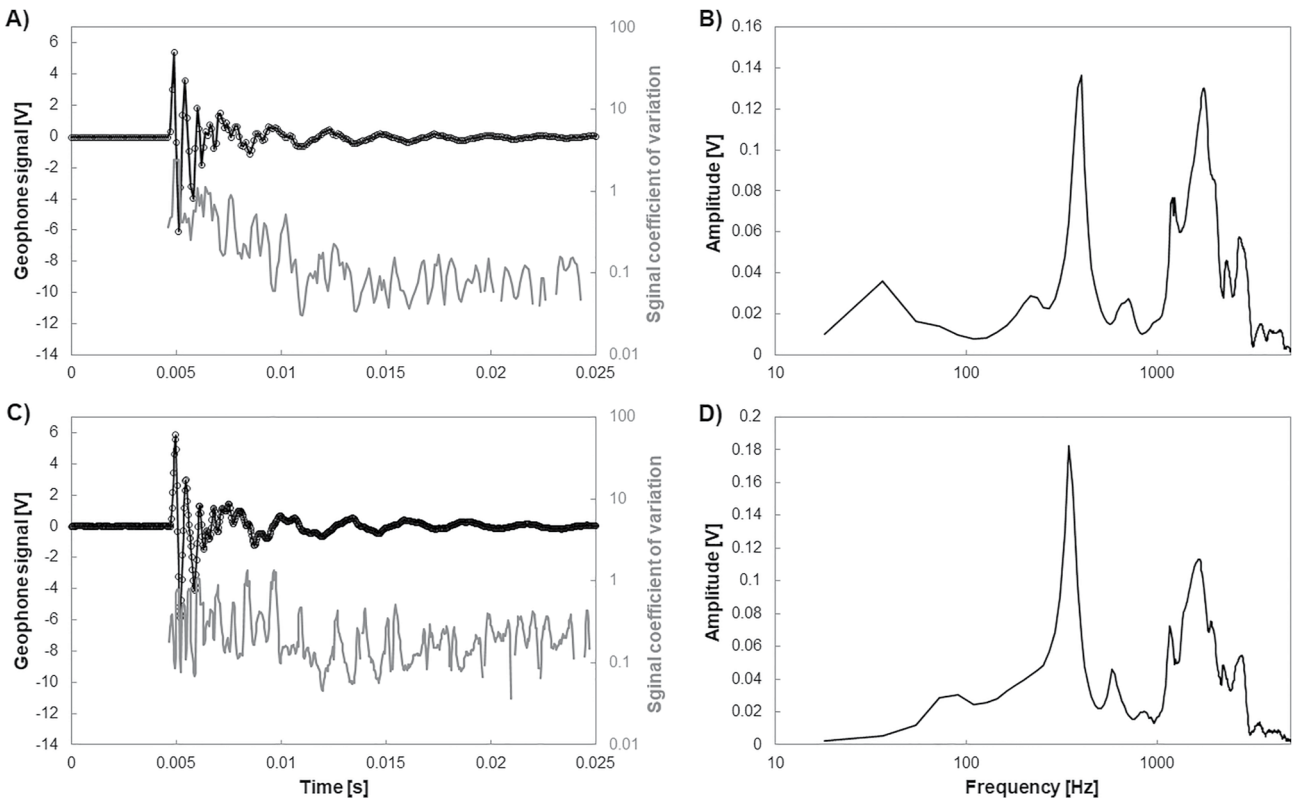

Figure 2. (a) and (c) average signal produced by eight replicas of single contacts of the metal sphere on the center of the plate and the associated coefficient of variability (gray curve). (b) and (d) average of the eight Fourier spectra computed for each replica. (a) and (b) signal recorded at 10 kHz; (c), (d) signal recorded at 30 kHz.

by the lower frequency of about 300–400 Hz. Impacts close to the plate edge show generally lower magnitude of oscillations and an almost complete disappearance of the frequency component in the 300–400 Hz range (Figure 3c).

From these analyses, it is possible to interpret the signal as formed by: (a) a first phase with high-frequency vibrations of the plate when hit by the sphere, which is rapidly damped; (b) followed by a second phase characterized by a more regular oscillation with a lower frequency in the range of 300–400 Hz that is related to the natural oscillatory frequency of the plate. The natural frequency of a steel plate with fixed edges can be estimated, knowing the dimensions of the plate, Young's elastic modulus (200 GPa), and Poisson's ratio (0.28). Following Gharaibeh and Obeidat (2018), the natural frequency of the considered plate is about 390 Hz. This is an approximate value, as it does not consider the presence of the screws and the weight of the attached geophone, but gives anyway a good approximation.

To further investigate the vibration modes of the plate, we tested different support configurations. Figures S1 and S2 in Supporting Information S1 show the results obtained with simply supported and fixed plates, with and without the elastomer. The analysis highlights that the role of the elastomer is to damp the maximum amplitude of the oscillations, and it does not change the fundamental mode of the plate vibration.

3.2. Dry Experiments

The dry experiments were designed to quantify the variability of the signal, when changing the point hit by the sphere. Each experiment was repeated 50 times.

Figure 4 shows the box plots of four different parameters, as a function of the distance of the impact point from the center of the plate, in both the transverse (358 mm) and the longitudinal (494 mm) plate directions. For all the four parameters (number of impulses, peak amplitude of the signal, power of the signal, and amplitude

10.1029/2022WR032116

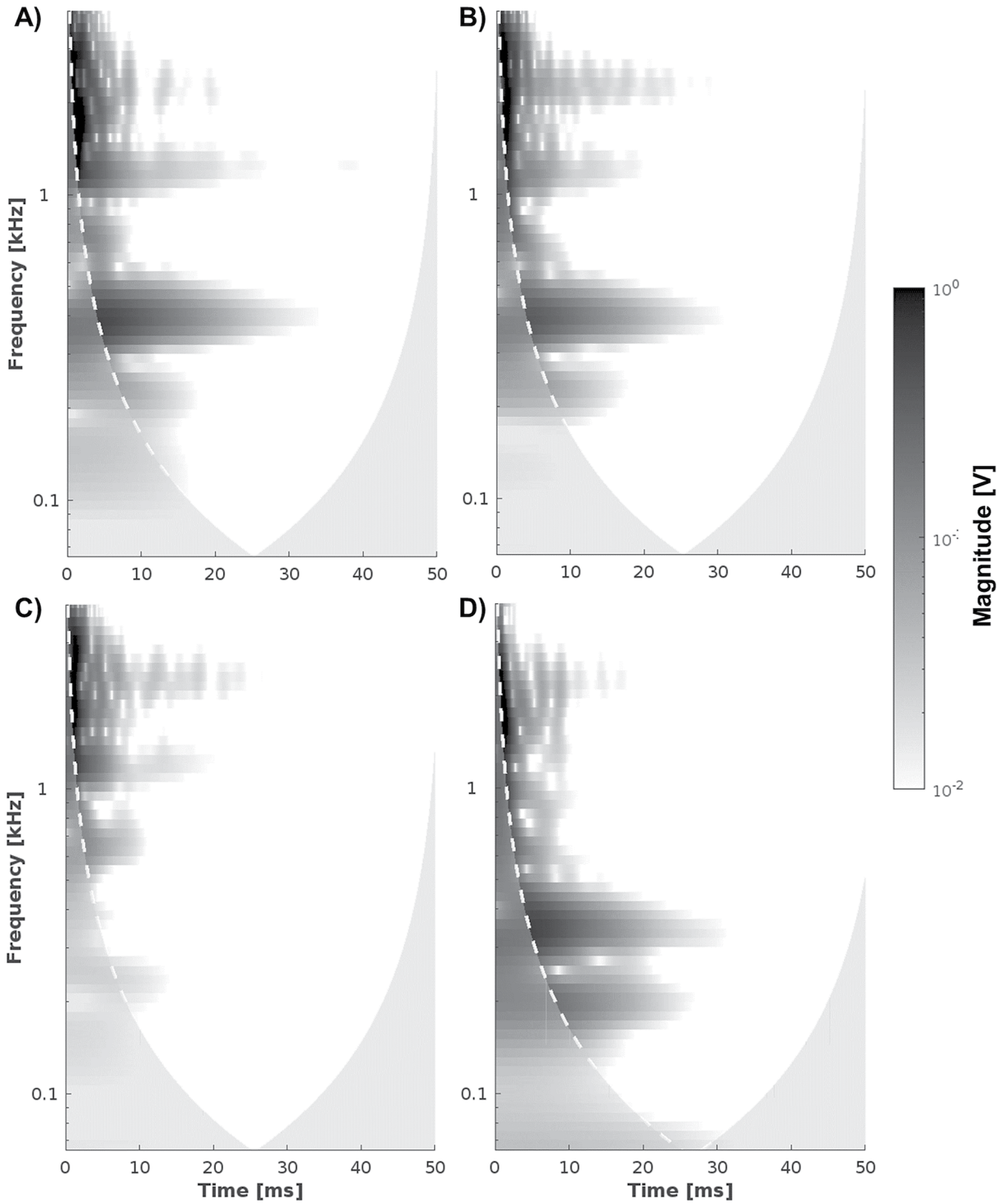

Figure 3. Examples of wavelet analysis of the 10 kHz signal for the sphere impacting: (a) the center of the plate; (b) a point 10 cm right of the plate center; (c) a point 20 cm right of the plate center. (d) Example of the wavelet analysis of the signal of particle 1 under flow conditions F1. Regions below the white dashed lines represent the cone of influence of the start and end points of the signal.

of the dominant harmonics in the range of 300–400 Hz, as obtained from the Fourier transform), there is a clear decreasing trend going from the plate center toward the edges. As expected from the relatively high coefficient of variability for the first phase recorded across multiple impacts (Figure 2a), the peak amplitude and the power of the signal are the more irregular ones of the four parameters. The number of impulses shows the largest variability

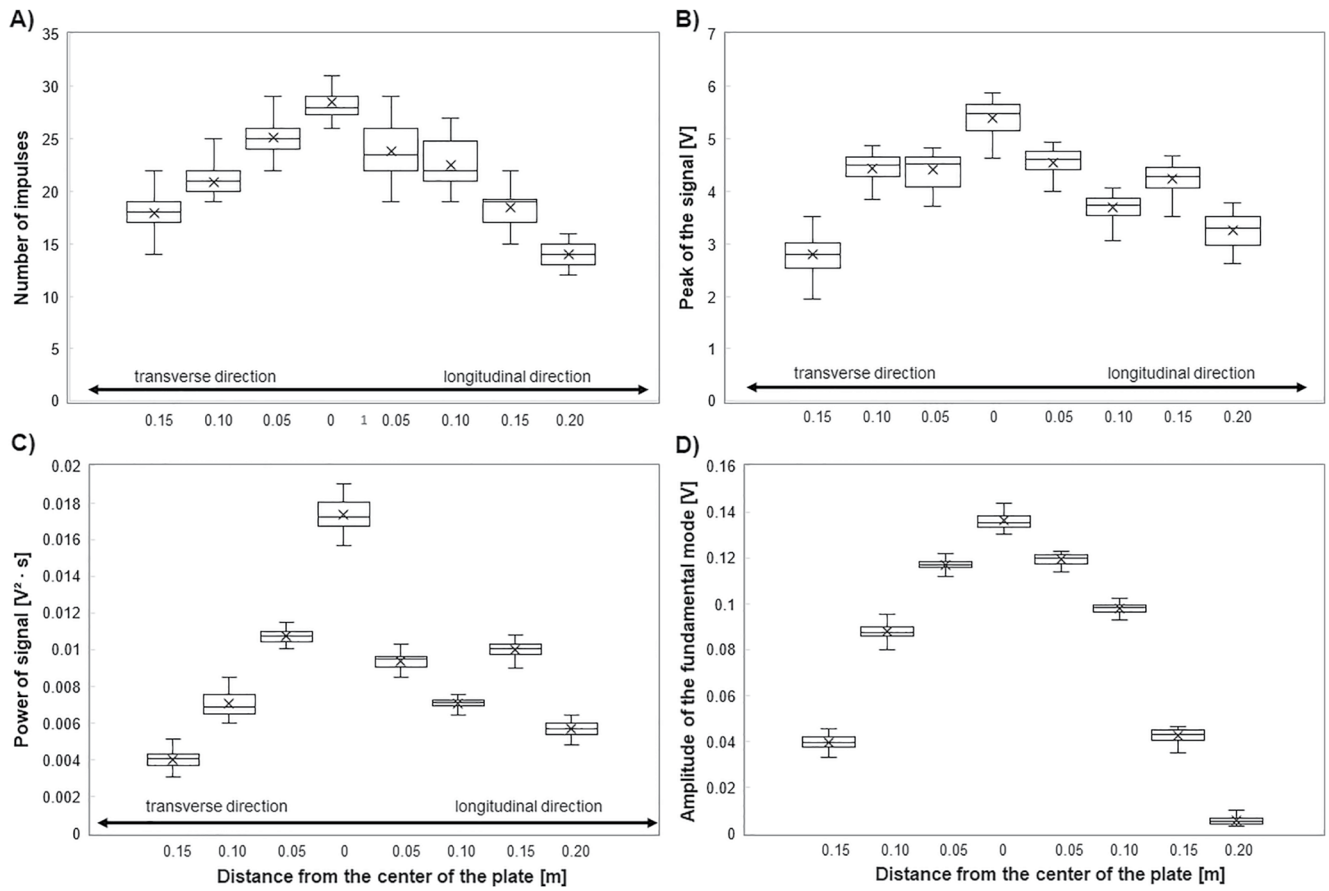

Figure 4. Box and whiskers plots of 50 replicas of identical hits of the metal sphere as a function of the distance of the hitting point from the plate center. (a) Number of impulses; (b) peak amplitude of the signal; (c) power of the signal; and (d) amplitude of the fundamental mode in the range of 300–400 Hz.

among identical replicas, with an interquartile range of about 10%–15% of the median. The amplitude of the fundamental mode in the range of 300–400 Hz appears as the least variable, with an interquartile range of about 3%–5% of the median for each impact point. This parameter also shows the clearest and most regular decreasing trend, with values decreasing by about 30% in the first 0.1 m and by about 70% at 0.15 m from the center.

This behavior is pointed out by the comparison of the Fourier spectra reported in Figure 5, where the average spectra over the 50 replicas are compared in the transverse direction of the plate. It is clear that the main difference is the gradual decrease of the peak in the range of 300–400 Hz, which disappears completely when the sphere hits a point on the edge of the plate. Although variable and noisy, the high-frequency components show peaks at similar frequencies, for different impact points.

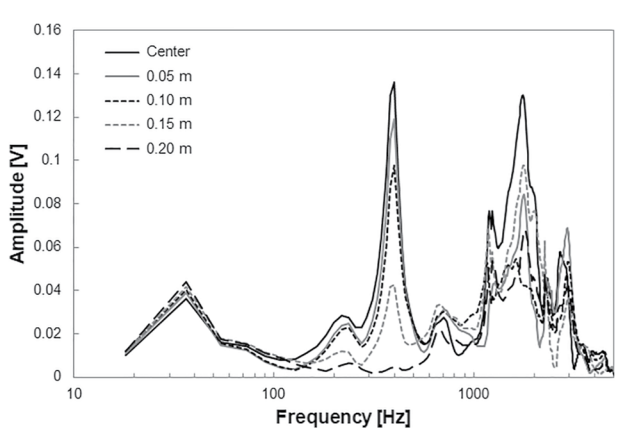

Figure 5. Comparison of the Fourier spectra for the different impact points along the transverse direction of the plate.

The spectra show that the 300–400 Hz vibration mode is the dominant mode when the sphere hits the plate within 0.1 m from the center. These observations suggest: (a) to use the amplitude of the fundamental mode as computed by the Fourier analysis as a parameter describing the geophone signal; (b) the possibility to filter only the impacts that occurred near the center of the plate based on the excitation of the fundamental mode of the plate (as determined through examination of the Fourier spectra).

3.3. Flow Experiments

Impacts generated during the flow experiments show similar characteristics, with a few notable differences. Specifically, the higher frequencies are even more rapidly damped, as highlighted by the wavelet analysis reported in

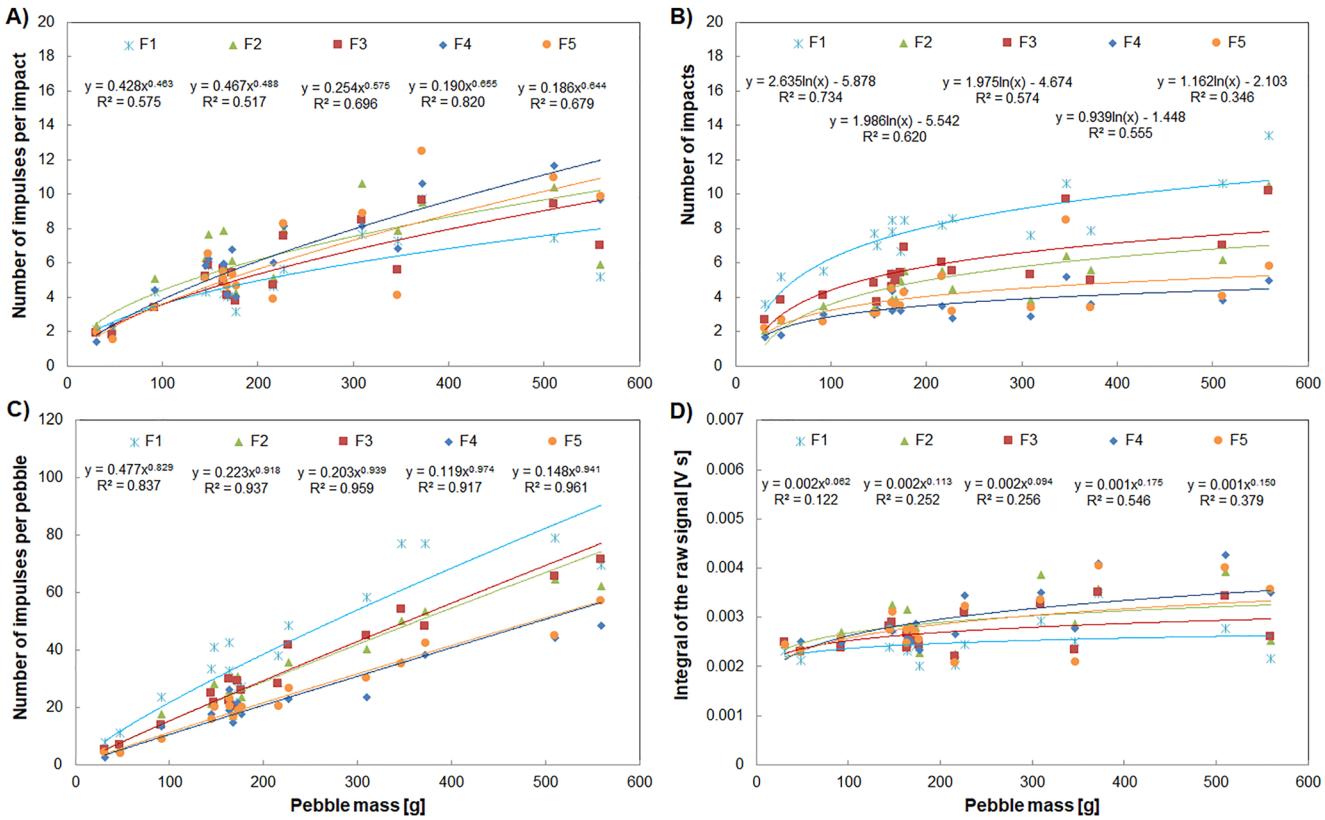

Figure 6. Average values on 10 replicated runs of (a) number of impulses per impact; (b) number of impacts per pebble; (c) number of impulses per pebble; and (d) integral of the module of each impulse, as a function of the mass of the pebble. Equation and R^2 of interpolation lines as power law (a, b, d) and logarithmic law (c) are reported on the top of each plot.

Figure 3d. Moreover, the fundamental mode has a slightly lower frequency than for the dry experiments, but it is always in the range of 300–400 Hz. This is probably caused by the damping effect of the water weight above the plate and further suggests to focus on the fundamental mode to interpret the signal.

Figure 6 reports the results of the flow experiments, as average values on 10 replicas for each pebble and as a function of its mass. Four parameters were analyzed, referring to the most commonly used in the literature. Figure 6a shows the number of impulses above the 0.1 V threshold, for each impact, whereas Figure 6b shows the average number of recorded impacts for each pebble. Interestingly, this latter parameter seems to be the one most affected by the flow conditions. The number of impacts decreases with increasing flow velocity and depth, but it is not possible to recognize a clear trend (see Table 2). Flow conditions in runs F1 determined a number of impacts more than double those for runs F4 and F5. As a result, also the number of impulses per each pebble (i.e., the product of the number of impulses per impact and the number of impacts) depends on the flow conditions (Figure 6c). This parameter, which is the one most used in practical applications (Rickenmann, 2017), has the strongest correlation with the pebble mass, with values of R^2 in the range of 0.84–0.96. It also shows a near linear relationship, with exponents of the power law in the range of 0.92–0.97. The integral of the signal (Figure 6d) shows the weakest correlation and a slightly positive relationship with flow velocity.

The intensity of the signal in terms of maximum amplitude of the raw signal and amplitude of the fundamental mode in the range of 300–400 Hz is reported in Figures 7a and 7b, respectively. Both these parameters show a good correlation with the pebbles mass; however, the amplitude of the dominant harmonics is the least affected by the flow conditions, with the five interpolation lines almost coincident. The analysis for all the parameters points out that there are four pebbles (4, 5, 10, and 17; Figure 1b and Table 1) that are invariably characterized by significantly lower values than would be expected given their masses. These four pebbles are the ones with the less spherical shape, as computed by the shape factor (Table 1). When removing the five pebbles with shape factor lower than 0.6 (with examples of both bladed and elongated pebbles), all the relationships improve

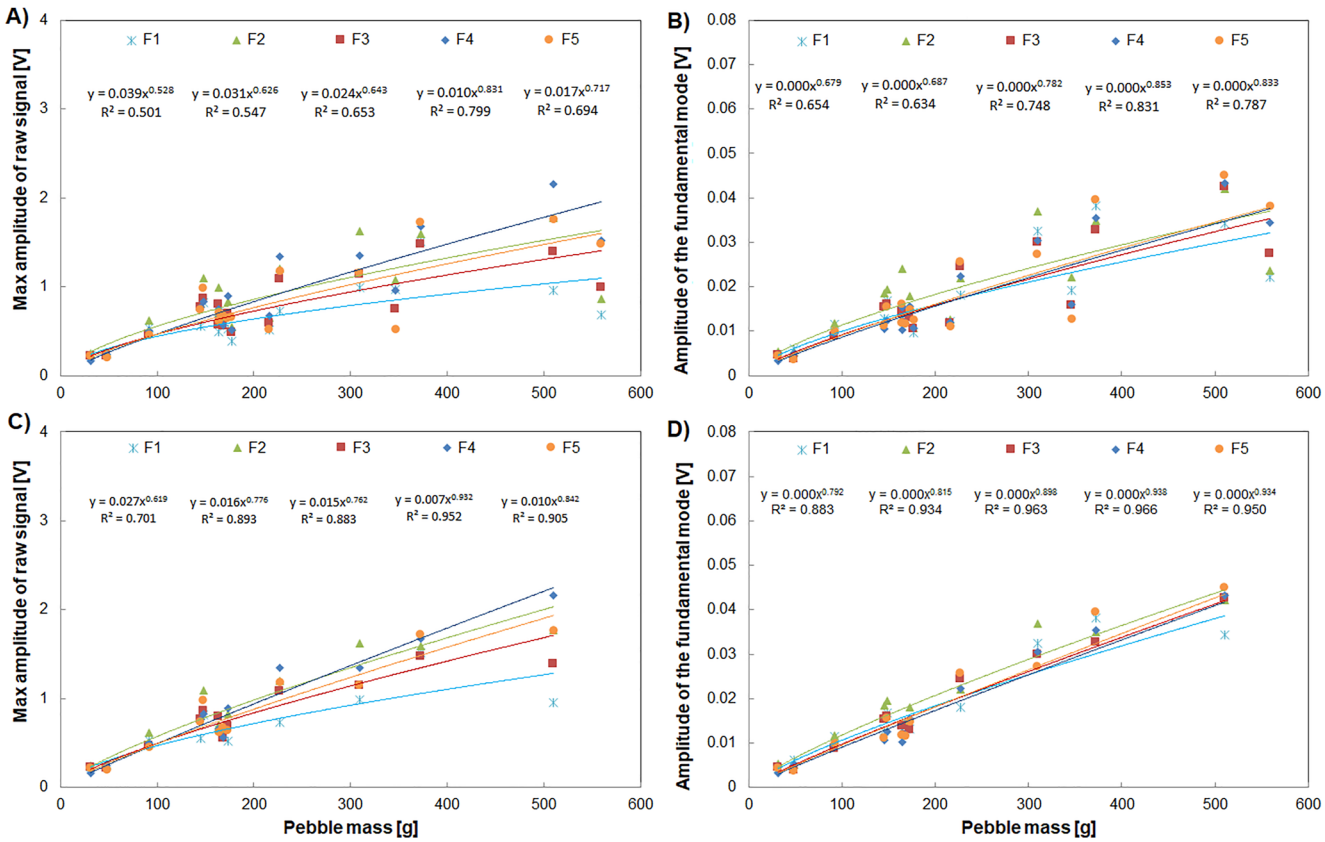

Figure 7. Average values on 10 replicated runs of (a) and (c) maximum amplitude of the raw signal; (b) and (d) amplitude of the fundamental mode in the range of 300–400 Hz. (a) and (b) All pebbles; (c) and (d) only pebbles with a shape factor larger than 0.6. Equation and R^2 of interpolation lines as power laws are reported on the top of each plot.

considerably. Figures 7c and 7d show the results for the maximum amplitude and the amplitude of the fundamental mode. Pebble number 7 has a shape factor slightly lower than 0.6, but plots in the same range as the more rounded pebbles, pointing out that more examples are needed to better define this behavior.

Along with the average behavior of each pebble, it is relevant to investigate the variability of the recorded signal. This is displayed in Figure 8, where the distributions of 50 runs for each pebble (10 replicas, 5 flow conditions) are plotted as a function of the pebble mass. The number of impulses per each impact and the amplitude of the fundamental mode in the 300–400 Hz range are shown. The variability is high, with the interquartile range (normalized by the median) reaching values of about 1 for both parameters and the range between the 10th and 90th percentiles (again normalized by the median) ranging between 1.5 and 2.5.

Supported by the results of the dry experiments, we filtered the impacts based on their Fourier spectrum to reduce the variability of the signal. Similarly to what we observed in the dry experiments, about half of the impacts are characterized by spectra with a very similar shape, which are not affected by the pebble size nor by the flow conditions, and show a dominant peak in the range of 300–400 Hz. The remaining half of the impacts is characterized by irregular Fourier spectra, with peaks at unpredictable frequencies, in many cases in the range of 1,000–3,000 Hz. These impacts are likely to occur on the edge of the plate, or when the pebble slides on the plate without a clear impact. We excluded all impacts whose Fourier spectrum (a) does not show the maximum amplitude in the range of 300–400 Hz and (b) has a total power after integrating across the range of 325–375 Hz that is less than 20% of that in the range of 0–600 Hz. These two criteria were calibrated to filter most of the impacts with a Fourier spectrum significantly different from the average one. As expected, this procedure mainly removed the impacts characterized by a below-average amplitude (comparing Figures 8b and 8d). The filtering does not change the overall trend, but it reduces the interquartile range (normalized with the median value) to approximately 0.85 (compared to 1 for the unfiltered data) and the range between the 10th and 90th percentiles from approximately 2 to 1.5, for both the number of impulses and the amplitude of the fundamental mode.

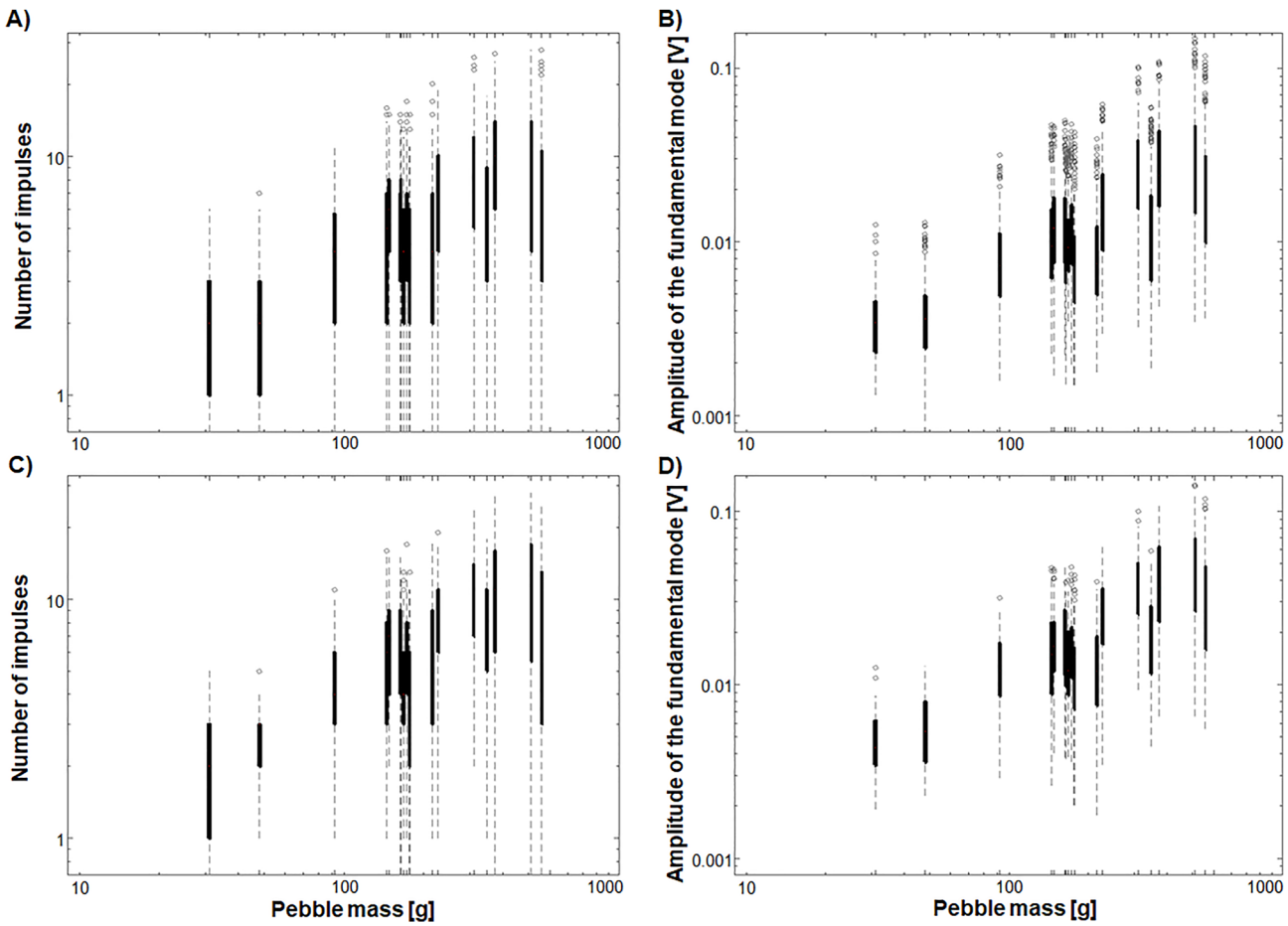

Figure 8. Box and whiskers plots of all the flow runs performed for each pebble, as a function of pebble mass. (a) and (c) Number of impulses per impact; (b) and (d) amplitude of the fundamental mode in the range of 300–400 Hz. (a) and (b) All impacts; (c) and (d) only impacts with a clear dominant peak in the 300–400 Hz range.

4. Discussion

4.1. Understanding the Vibration of the Geoplate

Geoplates have been installed in several gravel bed rivers to continuously monitor the bedload flux and its variability at seasonal or event time scales (Mao et al., 2016; Rickenmann, 2017). In many applications, the recorded seismic signal is immediately reduced to the number of impulses over a defined threshold per minute, to limit the amount of stored data and to allow for an easier data management. This approach has proven valid and gives relevant information on bedload flux, although more detailed data and elaborations are needed to improve our insight into bedload and its variability.

The method of quantifying the number of impulses was initially introduced for geophone signals obtained with the instrument installed directly in the ground (Govi et al., 1993; Hürlimann et al., 2003). In this configuration, seismic signals generated within the channel must propagate through the ground before being recorded by the geophone. Therefore, the vibration amplitudes and observed resonant frequencies are strongly dependent on both the geological structure around the geophone and the response of the ground between the impact and the geophone (Allstadt et al., 2020; Anthony et al., 2018; Arattano et al., 2014; Bakker et al., 2020). Active-source field calibrations need to be made to correct these factors. Using this approach, Bakker et al. (2020) were able to measure bedload flux in a gravel bed braided river with less than an order of magnitude uncertainty. In the case of the geoplate, the geophone is installed in a controlled setup, where the steel plate and the elastomer are similar in all configurations. This implies that the vibration modes of the plate are more regular and predictable. The analysis of the dry experiments reported in Sections 3.1 and 3.2 demonstrates that it is possible to take advantage of this setup to perform a more targeted signal analysis.

The observation that the plate vibrates mainly with a frequency equivalent to its fundamental mode in the range of 300–400 Hz, provides a more reliable way to characterize the impacts. The amplitude of this fundamental mode as computed by a Fourier Transform of the signal of each impact, seems to be the parameter better related to the mass of the hitting particle, and it is much less affected by the flow conditions compared to other common parameters (Figure 7). Higher frequencies (in the range of 1,000–2,500 Hz) are related to higher modes of vibration of the plate and characterize only the first 5 ms of the impact. These harmonics determine the maximum amplitude of the signal, but damp very rapidly and are more difficult to quantify with the standard 10 kHz acquisition rate. Our flume setup was characterized by a relatively smooth bed, meaning that in most mountain rivers, there could be different transport modes of the particles. This effect needs to be checked using larger experimental facilities (e.g., Nicollier, Antoniazza, Rieckenmann, et al., 2022) and field data. However, we do not expect this to change the general spectral response of the plate.

The occurrence of the fundamental mode in the 300–400 Hz range and its variability as a function of the hitting point is also useful to filter irregular impacts, caused by particles striking the border of the plate or simply sliding over it. These impacts determine a wide dispersion of the data, limiting the possibility to interpret the signal in terms of mass (or diameter) of the hitting particles. On the other hand, the proposed filtering will remove about half of the impacts, likely the ones generated by particles hitting the area close to the edges of the plate. This means that a linear array of multiple plates is not likely to monitor with the same accuracy the whole width of the riverbed. Calibration between the recorded signal and the total bedload flux will have to take this limitation into account.

Recent findings by Nicollier, Antoniazza, Rieckenmann, et al. (2022) showed that it is possible to filter the spurious vibrations generated by impacts on nearby plates and on the concrete sill surrounding the plates array checking the spectral characteristics of impacts. Particles directly impacting the plate always presented a first part of the impact with high frequencies (larger than 1 kHz), whereas spurious impacts caused the plate to vibrate predominantly with a frequency in the range of the fundamental mode. Combining these results with our observations, it looks like the different harmonics can be used in different ways to obtain the most from the signal, for example, using the occurrence of high frequencies to be sure the impact is not spurious, and then using the amplitude of the fundamental mode as a more robust parameter to characterize the mass of the impacting particle.

Results of our vibrational analysis have significant implications also for data acquisition and management, facilitating the development of onsite data elaboration procedures. This will improve the present most common situation, where only the number of impulses is stored. If data analysis is based on the fundamental mode in the 300–400 Hz range, the geophone signal could be sampled at a lower frequency, even down to 2 kHz, saving 80% of storage space with respect to the current 10 kHz standard acquisition rate. This will reduce the amount of stored data, while recording the entire signal, that is, most valuable information. Moreover, plate dimensions and material could be modified to obtain specific values of the fundamental mode, possibly further reducing the acquisition rate. It is worth noting that the standard Swiss plate geophone has a thickness of 15 mm, and therefore is expected to have a larger fundamental mode. The signal could than be analyzed to extract the single impacts, and from those the Fourier spectrum and the amplitude of the fundamental mode. This approach also needs to be tested under conditions of very intense bedload, when impacts may occur more frequently, possibly overlapping and therefore making the automatic recognition of single impacts more difficult. Considering the very short duration of impacts (about 30–40 ms), this should not be an issue for many flow conditions. The issue of signal saturation also exists for other metrics, as for the number of impacts and even more frequently for the amplitude of the raw signal, which could more easily exceed the 10 V limit. It is worth recalling that the amplitude of the fundamental mode in the 300–400 Hz is significantly lower than the maximum amplitude, as it represents the second phase of the plate vibration. Therefore the fundamental mode rarely saturates.

4.2. Geoplate Calibration

In the last years, research has been carried out to investigate whether it is possible to use a general calibration for the geoplate setup, limiting the need for direct bedload measurements, which are often expensive and time-consuming (Geay et al., 2020; Nicollier et al., 2021; Nicollier, Antoniazza, Ammann, et al., 2022; Wyss et al., 2016b). Our experiments in a controlled environment show that the total number of impulses generated by a pebble transported on the geoplate depends on the flow conditions, mainly by the increasing number of impacts when the flow velocity and depth are low. This means the calibration curve between impulses and

bedload rate needs to be adjusted taking into account the flow conditions, which vary both among sites and during floods. Recently, Nicollier, Antoniazza, Ammann, et al. (2022) showed that filtering the spurious impacts with an amplitude-frequency method results in more similar relationships between the number of impacts (packets) and the transported mass, across different field sites. Amplitudes of the 300–400 Hz harmonic signals are not significantly affected by flow conditions and therefore maybe more successfully used to derive a global calibration curve (e.g., Figure 7d). Our experiments involved only single particles, limiting the possibility to evaluate calibration curves that could be used in the field, which are generally derived for (many) impacts in time windows of minutes. Furthermore, our experiments pointed out an effect of particle shape on the geophone signal. This is in agreement with recent findings by Cassel et al. (2021), who showed a strong influence of particle shape on particle velocity and mean traveling distance. In particular, they showed that less rounded particles are more likely to be transported with a velocity up to three times lower than equal-sized spherical particles. Similarly, we observed lower amplitudes of impacts generated by elongated and platy particles, with values approximately half of those expected for particles of similar mass and rounded shape. The number of pebbles we used was not high enough to quantitatively evaluate the effect of particle shape and further research is needed on this issue.

Site-specific calibration is therefore require to take into account the variable particle shape as a function of lithology and the distance from the sediment source. In addition, there could be an effect at the flood scale, in case particles of different sizes or sources are mobilized during large floods.

4.3. Grain Size Estimation

Estimation of the grain size distribution of transported bedload from geoplates has been recently explored by Wyss et al. (2016a), Wyss et al. (2016c), and Nicollier et al. (2021). Their results from controlled experiments highlighted the possibility to infer grain size from signal amplitude and frequency. Our analysis confirmed the relationship with the amplitude of the signal, which depends on the mass (and in some way diameter) of the impacting pebble. However, the investigation of the vibration modes by means of the Fourier analysis showed that with our setup the frequency of the fundamental mode and of the higher harmonics does not depend on the pebble mass. An example of the averaged Fourier spectra for the 17 pebbles and flow conditions F1 is reported in Figure S3a in Supporting Information S1. Observed variations of the spectral centroid frequency, computed as the weighted mean of the frequencies in the signal, with their magnitudes as the weights, are more likely caused by a difference in the relative amplitude of the fundamental mode compared to the amplitude of higher modes (Figures S3b and S3c in Supporting Information S1). Higher vibration modes are characterized by a frequency in the range of 1,000–3,000 Hz, as also estimated by Wyss et al. (2016a). These modes show a much larger inherent variability, and are not easily measurable, because this vibration phase is very short (about 5 ms) and not always well reproduced with an acquisition rate of 10 kHz.

Wyss et al. (2016c), Nicollier, Antoniazza, Rieckenmann, et al. (2022), and Nicollier, Antoniazza, Ammann, et al. (2022) developed a procedure to estimate grain size from the spectral centroid frequency. In particular, Nicollier, Antoniazza, Ammann, et al. (2022) showed that after filtering the spurious impacts on other plates it is possible to obtain more consistent estimates of the particle size. Data in Figures 5 and 8 support the use of the frequency domain to filter the impacts in a further way, keeping only those that are more likely to be generated by a particle hitting the central area of the plate. In this way, the signal will be more clear and better related to the particle size, reducing the effect of particles impacting on the edge of the plate. These impacts are characterized by different spectra and therefore different amplitudes as well as centroid frequencies. Grain size could then be estimated by adding to the centroid frequency information about the amplitude of the fundamental mode, which shows a strong relationship with pebble mass and the lower sensitivity to flow conditions (see Figure 7). In any case, the observed large variability of the signal for replicas of runs with the same pebble suggests to use a statistical approach, quantifying the probability of each impact to be generated by a pebble of a specific grain size class.

As an example, in Figure 9, we computed the probability distributions of the amplitude of the fundamental mode (Figure 9a) and the centroid frequency (Figure 9b), for three sets of pebbles, classified in terms of mass (smaller than 50 g, larger than 200 g, and in between). The three distributions overlap significantly, meaning that, for example, an impact with amplitude of the fundamental mode equal to 0.01 V would have a probability of about 0.2 to be in the lightest or heaviest class, and 0.6 to be in the intermediate class. The distributions of the centroid frequency overlap even more, particularly for the two larger classes, suggesting that also considering information about the amplitude may improve the accuracy of the estimate.

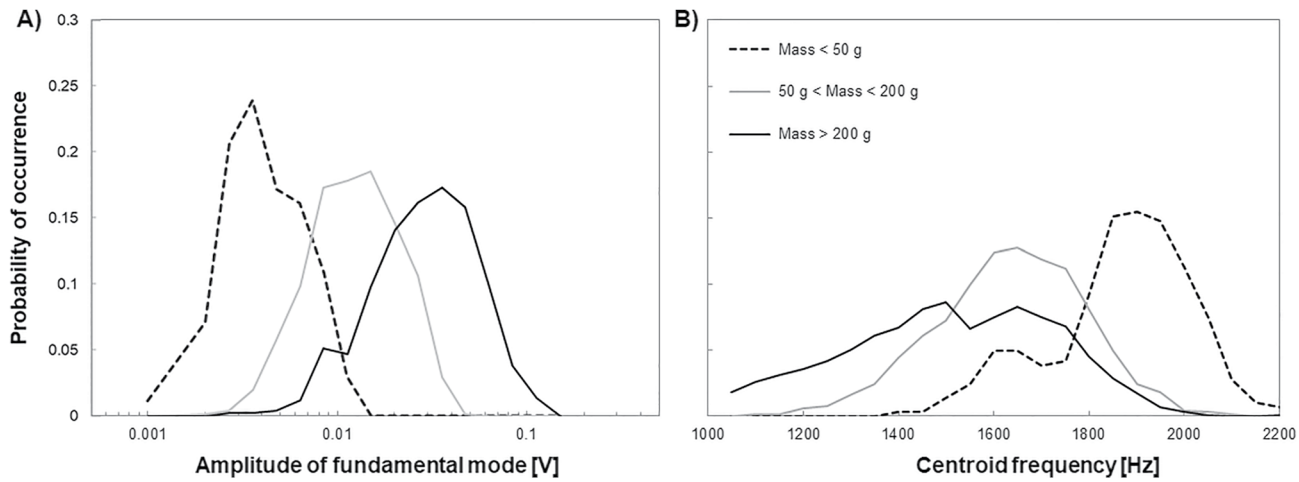

Figure 9. Probability distributions in terms of amplitude of (a) the fundamental mode and (b) the centroid frequency, for three classes of pebble mass.

Geoplates may therefore also be used to estimate the grain size distribution, although an absolute quantification still requires research and dedicated experiments. This technique could be more robustly used to evaluate changes of the grain size for different bedload events, thanks to continuous measurement, including at high flows. Difficulties in obtaining accurate estimations of sediment grain size have been highlighted also for indirect measurements with acoustic monitoring (Geay et al., 2020), suggesting that direct field measurements are so far the more reliable.

5. Conclusions

We performed two sets of experiments testing the vibration modes of the geoplate. Signal analysis showed that there are two distinct phases in the recorded signal. The first one lasts for less than 5 ms and is characterized by higher frequencies and larger amplitudes. The second one is related to the fundamental frequency of the plate; it is characterized by a lower frequency in the range of 300–400 Hz and by an amplitude that is consistent among replicas.

Dry experiments with a metal sphere hitting different points on the plate emphasized how the signal changes as a function of the distance from the plate center. This highlights that the central zone of the plate is more sensitive to bedload. This zone is approximately a circle with a diameter of 0.2–0.3 m.

Flow experiments showed that the number of impacts for each pebble is largely affected by the flow conditions (and particle shape), whereas parameters of the single impact are not, depending mainly on the mass of the hitting particle. These results suggest that a full recording of the signal even at lower frequency such as 2 kHz, coupled with an automatic recognition of single impacts and an FFT analysis, can improve the quantification of the bedload flux, and may allow for interpreting the signal also in terms of grain size distribution. On the other hand, the observed variability of the number of impacts as a function of the flow conditions and the particle shape points out that a precise calibration of the geoplate is likely to remain site-specific.

Acknowledgments
MP, SS, and GV acknowledge support from the project SEDIPLAN—"Sediment budgeting and planning for rivers in South-Tyrol, from hazard mitigation to environmental restoration" funded by the European Regional Development Fund (ERDF) and by the Autonomous Province of Bolzano/Bozen (FESR1003). WB acknowledges support from the project GLORI—Glaciers-to-Rivers Sediment Transfer in Alpine Basins (project no. 42), funded by the Autonomous Province of Bolzano/Bozen. The paper has benefited greatly from the comments and suggestions by the associate editor, David Gaeuman and Robert Anthony, who also helped interpreting plate vibrations. Open Access Funding provided by Università degli Studi di Trento within the CRUI-CARE Agreement.

Data Availability Statement

Raw data used in this paper can be accessed at https://doi.org/10.5281/zenodo.5873658 (Portogallo et al., 2022).

References

Allstadt, K., Farin, M., Iverson, R., Obryk, M., Kean, J., Tsai, V., et al. (2020). Measuring basal force fluctuations of debris flows using seismic recordings and empirical green's functions. *Journal of Geophysical Research: Earth Surface*, *125*(9), e2020JF005590. https://doi.org/10.1029/2020JF005590

Anthony, R., Aster, R., Ryan, S., Rathburn, S., & Baker, M. (2018). Measuring mountain river discharge using seismographs emplaced within the hyporheic zone. *Journal of Geophysical Research: Earth Surface*, *123*(2), 210–228. https://doi.org/10.1002/2017JF004295

Antoniazza, G., Nicollier, T., Wyss, C., Boss, S., & Rickenmann, D. (2020). Bedload transport monitoring in alpine rivers: Variability in Swiss plate geophone response. *Sensors*, *20*, 4089. https://doi.org/10.3390/s20154089

Arattano, M., Abancó, C., Coviello, V., & Hürlimann, M. (2014). Processing the ground vibration signal produced by debris flows: The methods of amplitude and impulses compared. *Computers & Geosciences*, *73*, 17–27. https://doi.org/10.1016/j.cageo.2014.08.005

Bakker, M., Gimbert, F., Geay, T., Misset, C., Zanker, S., & Recking, A. (2020). Field application and validation of a seismic bedload transport model. *Journal of Geophysical Research: Earth Surface*, *125*(5), e2019JF005416. https://doi.org/10.1029/2019jf005416

Barrière, J., Krein, A., Oth, A., & Schenkluhn, R. (2015). An advanced signal processing technique for deriving grain size information of bedload transport from impact plate vibration measurements. *Earth Surface Processes and Landforms*, *40*(7), 913–924. https://doi.org/10.1002/esp.3693

Belleudy, P., Valette, A., & Benjamin, G. (2010). *Passive hydrophone monitoring of bedload in river beds: First trials of signal spectral analyses*. U.S. Geological Survey Scientific Investigations Report.

Cassel, M., Lavé, J., Recking, A., Malavoi, J., & Piégay, H. (2021). Bedload transport in rivers, size matters but so does shape. *Scientific Reports*, *11*, 508. https://doi.org/10.1038/s41598-020-79930-7

Geay, T., Zanker, S., Misset, C., & Recking, A. (2020). Passive acoustic measurement of bedload transport: Toward a global calibration curve? *Journal of Geophysical Research: Earth Surface*, *125*, e2019JF005242. https://doi.org/10.1029/2019jf005242

Gharaibeh, M., & Obeidat, A. (2018). Vibrations analysis of rectangular plates with clamped corners. *Open Engineering*, *8*(1), 275–283. https://doi.org/10.1515/eng-2018-0030

Govi, M., Maraga, F., & Moia, F. (1993). Seismic detectors for continuous bed load monitoring in a gravel stream. *Journal des Sciences Hydrologiques*, *38*, 123–132. https://doi.org/10.1080/02626669309492650

Gray, J., Laronne, J., & Marr, J. (2010). *Bedload-surrogate monitoring technologies (Scientific investigations report No. 2010–5091)*. US Geological Survey.

Hürlimann, M., Rickenmann, D., & Graf, C. (2003). Field and monitoring data of debris-flow events in the Swiss Alps. *Canadian Geotechnical Journal*, *40*, 161–175. https://doi.org/10.1139/t02-087

Mao, L., Carrillo, R., Escaurazia, C., & Iroume, A. (2016). Flume and field-based calibration of surrogate sensors for monitoring bedload transport. *Geomorphology*. https://doi.org/10.1016/j.geomorph.2015.10.002

Mizuyama, T., Laronne, J., Nonaka, M., Sawada, T., Satofuka, Y., Matsuoka, M., et al. (2010). Calibration of a passive acoustic bedload monitoring system in Japanese mountain rivers. In J. Gray, J. Laronne, & J. Marr (Eds.), *US Geological Survey Scientific Investigations Report 2010-5091* (pp. 296–318). US Geological Survey.

Nicollier, T., Antoniazza, G., Ammann, L., Rieckenmann, D., & Kirchner, J. (2022). Toward a general calibration of the Swiss plate geophone system for fractional bedload transport. *Earth Surface Dynamics Discussions*. https://doi.org/10.5194/esurf-2022-7

Nicollier, T., Antoniazza, G., Rieckenmann, D., Hartlieb, A., & Kirchner, J. (2022). Improving the calibration of the Swiss plate geophone bedload monitoring system by filtering out seismic signals from extraneous particle impacts. *Earth and Space Science*, *9*, e2021EA001962. https://doi.org/10.1029/2021ea001962

Nicollier, T., Rieckenmann, D., & Hartlieb, A. (2021). Field and flume measurements with the impact plate: Effect of bedload grain-size distribution on signal response. *Earth Surface Processes and Landforms*, *46*, 1504–1520. https://doi.org/10.1002/esp.5117

Petrut, T., Geay, T., Gervaise, C., Belleudy, P., & Zanker, S. (2018). Passive acoustic measurement of bedload grain size distribution using self-generated noise. *Hydrology and Earth System Sciences*, *22*(1), 767–787. https://doi.org/10.5194/hess-22-767-2018

Portogallo, M., Simoni, S., Vignoli, G., & Bertoldi, W. (2022). Experimental data of geoplate bedload signal of single pebbles [Dataset]. Zenodo. https://doi.org/10.5281/zenodo.5873658

Recking, A., Liébault, F., Peteuil, C., & Jolimet, T. (2010). Testing bedload transport equations with consideration of time scales. *Earth Surface Processes and Landforms*, *37*, 774–789. https://doi.org/10.1002/esp.3213

Rennie, C., Millar, R., & Church, M. (2002). Measurement of bed load velocity using an acoustic Doppler current profiler. *Journal of Hydraulic Engineering*, *128*(5), 473–483. https://doi.org/10.1061/(asce)0733-9429(2002)128:5(473)

Rickenmann, D. (2017). Bed-load transport measurements with geophones and other passive acoustic methods. *Journal of Hydraulic Engineering*, *143*(6), 03117004-1. https://doi.org/10.1061/(asce)hy.1943-7900.0001300

Rickenmann, D., & McArdell, B. (2007). Continuous measurement of sediment transport in the Erlenbach stream using piezoelectric bedload impact sensors. *Earth Surface Processes and Landforms*, *32*(9), 1362–1378. https://doi.org/10.1002/esp.1478

Rickenmann, D., Turowski, J. M., Fritschi, B., Klaiber, A., & Ludwi, A. (2012). Bedload transport measurements at the Erlenbach stream with geophones and automated basket samplers. *Earth Surface Process and Landforms*, *37*, 1000–1011. https://doi.org/10.1002/esp.3225

Schmandt, B., Aster, R., Scherler, D., Tsai, V., & Karlstrom, K. (2013). Multiple fluvial processes detected by riverside seismic and infrasound monitoring of a controlled flood in the Grand Canyon. *Geophysical Research Letters*, *40*(18), 4858–4863. https://doi.org/10.1002/grl.50953

Soar, P., & Downs, P. (2017). Estimating bedload transport rates in a gravel-bed river using seismic impact plates: Model development and application. *Environmental Modelling & Software*, *90*, 182–200. https://doi.org/10.1016/j.envsoft.2017.01.012

Tsakiris, A. G., Papanicolaou, A. N., Goodrich, H., & Lauth, T. J. (2014). Signature of bedload particle transport mode in the acoustic signal of a geophone. *Journal of Hydraulic Research*, *52*(2), 185–204. https://doi.org/10.1080/00221686.2013.876454

Tsubaki, R., Kawahara, Y., Zhang, X.-H., & Tsuboshita, K. (2017). A new geophone device for understanding environmental impacts caused by gravel bedload during artificial floods. *Water Resources Research*, *53*, 1491–1508. https://doi.org/10.1002/2016wr019726

Vericat, D., Church, M., & Batalla, R. (2006). Bed load bias: Comparison of measurements obtained using two (76 and 152 mm) Helley-smith samplers in a gravel bed river. *Water Resources Research*, *42*, W01402. https://doi.org/10.1029/2005wr004025

Wilcock, P. (2001). Toward a practical method for estimating sediment-transport rates in gravel-bed rivers. *Earth Surface Processes and Landforms*, *26*, 1395–1408. https://doi.org/10.1002/esp.301

Wyss, C., Rickenmann, D., Fritschi, B., Turowski, J., Weitbrecht, R., & Boes, V. (2016a). Laboratory flume experiments with the Swiss plate geophone bed load monitoring system: 1. Impulse counts and particle size identification. *Water Resources Research*, *52*(10), 7744–7759. https://doi.org/10.1002/2015wr018555

Wyss, C., Rickenmann, D., Fritschi, B., Turowski, J., Weitbrecht, R., & Boes, V. (2016b). Laboratory flume experiments with the Swiss plate geophone bed load monitoring system: 2. Application to field sites with direct bed load samples. *Water Resources Research*, *52*(10), 7760–7778. https://doi.org/10.1002/2016wr019283

Wyss, C., Rickenmann, D., Fritschi, B., Turowski, J., Weitbrecht, R., & Boes, V. (2016c). Measuring bedload transport rates by grain size fraction using the Swiss plate geophone signal at the Erlenbach. *Journal of Hydraulic Engineering*, *142*(5), 04016003. https://doi.org/10.1061/(asce)hy.1943-7900.0001090